16TH EUROPEAN CONFERENCE ON EARTHQUAKE ENGINEERING THESSALONIKI 18 - 21 JUNE 2018

NUMERICAL INVESTIGATION OF MASONRY STRUCTURES ON THE MICRO LEVEL

Shenghan ZHANG[1], Nicolas RICHART[2], Katrin BEYER[3]

ABSTRACT

The force-displacement behavior of stone masonry elements depends on the properties of their constituents, mortar and stone, as well as on their typology, i.e., the shape and size of the stones and the patterns they generate. It is well known that stone masonry typology depends on geographical regions, construction periods, and building technology. However, relatively few research has been dedicated to study its influence on the mechanical properties of the stone masonry. Existing studies used experimental tests in order to investigate the stone masonry pattern. However, such studies are often rather small due to the considerable costs associated to experimental tests. Furthermore, it is often difficult to change all parameters systematically. For this reason, this study uses a numerical approach, which requires a detailed micro-modeling method and a typology generator to systematically generate masonry patterns. The objective of this research is to investigate the mechanical behavior of different typologies.

This study builds upon a detailed micro-modeling approach with cohesive elements and a newly developed micro-structure generator. Samples of different typologies are subjected to two different boundary conditions, compression and shear compression. For the shear compression tests, two compression levels are applied, under which specimens exhibit a flexural and a mixed failure mode, respectively. Depending on the failure mode, a significant influence of typology on the mechanical behavior of masonry elements is observed. More specifically, there is a significant positive correlation between line of minimum trace and compressive/shear strength. This research outlines how the detailed micro-modeling technique in combination with a typology generator can be used to systematically investigate the influence of stone masonry topology on the mechanical behavior and lays the foundation for future studies.

Keywords: Historical masonry; Detailed micro-modeling; Typology generator; Line of minimum trace; Cohesive zone model

1. INTRODUCTION

Stone masonry is one the oldest construction materials and can be found in many of today's cultural heritage structures. Stone masonry buildings are also among the most vulnerable structures under earthquake loading (D'Ayala and Speranza 2003; Grünthal 1993). Effectively planning strengthening interventions that preserve the appearance and fabric of such cultural heritage structures requires a good understanding of their seismic behavior. However, understanding the mechanical behavior of stone masonry elements is a long-standing challenge in civil engineering (Roca et al. 2010). The force-displacement behavior of stone masonry elements depends on the properties of their constituents, mortar and stone, as well as on their typology, i.e., the shape and size of the stones and the patterns they generate. This paper focuses on the influence of the latter, masonry typology.

Previously, experimental research was used to quantify the differences between stone masonry

[1] PhD student, Earthquake Engineering and Structural Dynamics (EESD), IIC, ENAC, Ecole Polytechnique Fédérale de Lausanne (EPFL), Switzerland. shenghan.zhang@epfl.ch

[2] Senior scientist, Earthquake Engineering and Structural Dynamics (EESD), IIC, ENAC, Ecole Polytechnique Fédérale de Lausanne (EPFL), Switzerland. nicolas.richart@epfl.ch

[3] Associate professor, Earthquake Engineering and Structural Dynamics (EESD), IIC, ENAC, Ecole Polytechnique Fédérale de Lausanne (EPFL), Switzerland. katrin.beyer @epfl.ch

typologies (Kržan et al. 2015; Vanin et al. 2017). However, the substantial variety of stone masonry topologies and the difficulty of controlling certain parameters in the laboratory (e.g. stone shape, stone size distribution, distribution of material properties within the element) call for numerical simulations in which parameters can be varied systematically and many analyses can be conducted.
When modelling masonry elements, three levels of detail are normally distinguished, i.e., macro-modeling, simplified micro-modeling, and detailed micro-modeling. Macro-modeling is by far the most common strategy for engineering practice. It treats masonry as a homogeneous material (Milani et al. 2006) and often replies on experimental tests to provide necessary information for the material model. Methods that can account explicitly for the masonry pattern are the simplified micro-model (Senthivel and Louren ço 2009) and the detailed micro-model (Pina-Henriques 2005; Shieh-Beygi and Pietruszczak 2008; Vandoren et al. 2013; Zhang et al. 2017b). In the former, mortar joints are modeled as zero-thickness interface elements while in the latter, mortar, units and (sometimes) interface are modeled explicitly. With the advent of advanced numerical model and the increase of computational power, the detailed micro-modeling approach is becoming more and more popular. The simulation strategy adopted in this paper is based on our previous work on the detailed micro-modeling approach with cohesive elements (the numerical formulation is summarized in Section 2), which has the advantage of explicitly representing cracks and interfacial damage.
In order to study the influence of masonry typology, another cornerstone that was missing was the ability to systematically generate patterns for different masonry typologies. While the calibration of brick masonry typology is easy and some related research on interlocking exists, generation of stone masonry pattern is much more difficult. To this end, we resort to a newly proposed micro-structure generator (Zhang et al. 2017a). The basic procedure is summarized in Section 3. For each typology, three samples are generated, and material strengths are obtained under different boundary conditions. The correlation between material strength and the line of minimum trace is then discussed.

2. NUMERICAL FRAMEWORK

Starting with the well-known weak form of the virtual work principle

$$\int_V \mathbf{P}\colon \mathbf{E} dV_0 + \int_V \rho_0 \boldsymbol{b} \cdot \delta \boldsymbol{u} dV_0 + \int_{S_f} \boldsymbol{t} \cdot \delta \boldsymbol{u} dS_0 + \int_V \rho_0 \ddot{\boldsymbol{u}} \cdot \delta \boldsymbol{u} dV_0 - \int_{S_{intf}} \boldsymbol{T} \cdot \left[[\delta \boldsymbol{u}]\right] = 0 \tag{1}$$

in which the V and S_f refer to volume and Newmann boundary of the body, $\boldsymbol{P}$ is the first Piola–Kirchhoff stress, $\boldsymbol{E}$ is the Green strain, ρ_0 is the density of the material, $\boldsymbol{b}$ is the body force, $\delta \boldsymbol{u}$ is the virtual displacement, $\boldsymbol{t}$ is the Newmann boundary condition applied on S_f, $\left[[\cdot]\right]$ indicates the jump of displacement across cohesive elements and $\boldsymbol{T}$ represents the cohesive traction along the interface S_{intf}. The symbol : indicates the inner product between second order tensors. After spatial discretization, the following well-known relationship is obtained:

$$\mathbf{M}\ddot{\boldsymbol{u}} + \boldsymbol{f}^{\text{int}} = \boldsymbol{f}^{\text{ext}} \tag{2}$$

in which $\mathbf{M}$ is the mass matrix, $\ddot{\boldsymbol{u}}$ is the acceleration vector, $\boldsymbol{f}^{\text{int}}$ and $\boldsymbol{f}^{\text{ext}}$ are internal and external force vectors. The classical explicit second order central difference method is used here for time integration. The displacement, velocity, acceleration ($\boldsymbol{u}_{m+1}$, $\dot{\boldsymbol{u}}_{m+1}$, $\ddot{\boldsymbol{u}}_{m+1}$) at time step $m+1$ is estimated by

$$\boldsymbol{u}_{m+1} = \boldsymbol{u}_m + \Delta t \dot{\boldsymbol{u}}_m + \frac{1}{2}\Delta t^2 \ddot{\boldsymbol{u}}_m \tag{3}$$

$$\ddot{\boldsymbol{u}}_{m+1} = \mathbf{M}^{-1}(\boldsymbol{f}^{\text{ext}}_{m+1} - \boldsymbol{f}^{\text{int}}_{m+1}) \tag{4}$$

$$\dot{\boldsymbol{u}}_{m+1} = \dot{\boldsymbol{u}}_m + \frac{1}{2}\Delta \text{t}(\ddot{\boldsymbol{u}}_{m+1} + \ddot{\boldsymbol{u}}_m) \tag{5}$$

A constant time step Δt is used during the simulation, which is confined by

$$\Delta t < \Delta t_{\text{stable}} = \alpha \frac{l_{\min e}}{c_l} \tag{6}$$

in which c_l represents the longitudinal wave speed, $l_{\min e}$ is the characteristic length of the minimum element, α is a safety factor, chosen to be 0.15 here.

Calculating $\boldsymbol{f}^{\text{int}}$ requires a constitutive law for the bulk elements and a traction-separation law for cohesive element. For bulk elements, an isotropic elastic relation is assumed. Material nonlinearity comes from cohesive elements. Here the extrinsic approach (Camacho and Ortiz 1996) is used, for which cohesive elements are inserted dynamically during the simulation while the following criteria is met

$$\sigma^{\text{eff}} > \sigma_c \tag{7}$$

in which σ_c is the critical stress, σ^{eff} is the effective stress for the current stress state calculated by (Camacho and Ortiz 1996)

$$\sigma^{\text{eff}} = \begin{cases} \sqrt{t_n^2 + \dfrac{t_\tau^2}{\beta^2}} \ \text{for tension/shear } t_n \geq 0 \\ \dfrac{1}{\beta} \cdot (|t_\tau| - \mu |t_n|) \ \text{for compression/shear } t_n < 0 \end{cases} \tag{8}$$

in which $t_n = \boldsymbol{\sigma} \cdot \boldsymbol{n}$, $t_\tau = \boldsymbol{\sigma} \cdot \boldsymbol{\tau}$ are the tractions at the normal direction $\boldsymbol{n}$ and tangential direction $\boldsymbol{\tau}$ of the facets, β is the shear stress factor, μ is the friction coefficient. Two situations, tension/shear $\sigma_n \geq 0$ and compression/shear $\sigma_n < 0$, are distinguished,

After insertion, the traction is determined by the traction-separation law. The following traction-separation law is used (Snozzi and Molinari 2013)

$$\boldsymbol{T} = \left(\frac{\beta^2}{\kappa} \delta_t \boldsymbol{\tau} + \delta_n \boldsymbol{n} \right) T \tag{9}$$

in which $\kappa = G_{c,II}/G_{c,I}$, β indicate the ratio between cohesion and tensile strength, T is a scalar value determined by

$$T = \begin{cases} \sigma_c \left(1 - \dfrac{\delta}{\delta_c} \right) \ \text{for opening } \delta = \delta_{max} \\ \dfrac{\delta}{\delta_{max}} T_{max} \ \text{for closing/reopening } \delta < \delta_{max} \end{cases} \tag{10}$$

where $\delta_c = 2G_{c,I}/\sigma_c$ represents the effective separation upon which the cohesive element is totally damaged, δ_{max} is the maximum effective separation. The effective separation is calculated by (Snozzi and Molinari 2013)

$$\delta = \sqrt{\frac{\beta^2}{\kappa^2} \delta_t^2 + \delta_n^2} \tag{11}$$

For contact, we use the same node-to-node contact in Zhang et al. (2017b), in which the contact and friction forces, $f_{cont,ij}^m$ and $f_{fric,ij}^m$, at time step m for node pair i, j is calculated by prediction of the displacement at time step $m + 1$, more specifically

$$\delta u_{ij}^{p} = \left(\widehat{\boldsymbol{u}}_i^{m+1} - \widehat{\boldsymbol{u}}_j^{m+1}\right) \cdot \boldsymbol{n} \tag{12}$$

$$f_{cont,ij}^{m} = \frac{\delta u_{ij}^{p}}{\Delta t^2 \left(\frac{1}{m_i} + \frac{1}{m_j}\right)} \tag{13}$$

$$f_{fric,ij}^{m} = \min\left(\mu f_{cont,ij}^{m}, \left|\frac{2\left(\widehat{\boldsymbol{u}}_i^{m+1} - \widehat{\boldsymbol{u}}_j^{m+1}\right) \cdot \boldsymbol{\tau}}{\Delta t \left(\frac{1}{m_i} + \frac{1}{m_j}\right)}\right|\right) \tag{14}$$

where $\widehat{\boldsymbol{u}}_i^{m+1}$, $\widehat{\boldsymbol{u}}_j^{m+1}$, $\widehat{\boldsymbol{u}}_i^{m+1}$, $\widehat{\boldsymbol{u}}_j^{m+1}$ are unconstraint displacements and velocities predicted at time step $m+1$, m_i and m_j are the lumped masses for the node pair i, j which comes in contact.

3. TYPOLOGY GENERATOR AND LINE OF MINIMUM TRACE

"Stone masonry" is a very general term. The form of stone masonry ranges from regular block masonry to irregular rubble masonry. Here in this section, we summarize the basic idea of our recently proposed typology generator; more detailed information can be found in Zhang et al. (2017a).

3.1 Classification of Masonry Topologies

Due to the large variation of stone masonry, it is more practical to categorize them. In Italian code (MIT 2009), five different categories are distinguished. The visualization of these categories, listed below in Figure 1, is originally given in Vanin et al. (2017). From typology A to typology E, the masonry goes from total irregular to regular (other criteria used for distinguishing different typologies, e.g., material used, interlocking in the thickness direction, are omitted here).

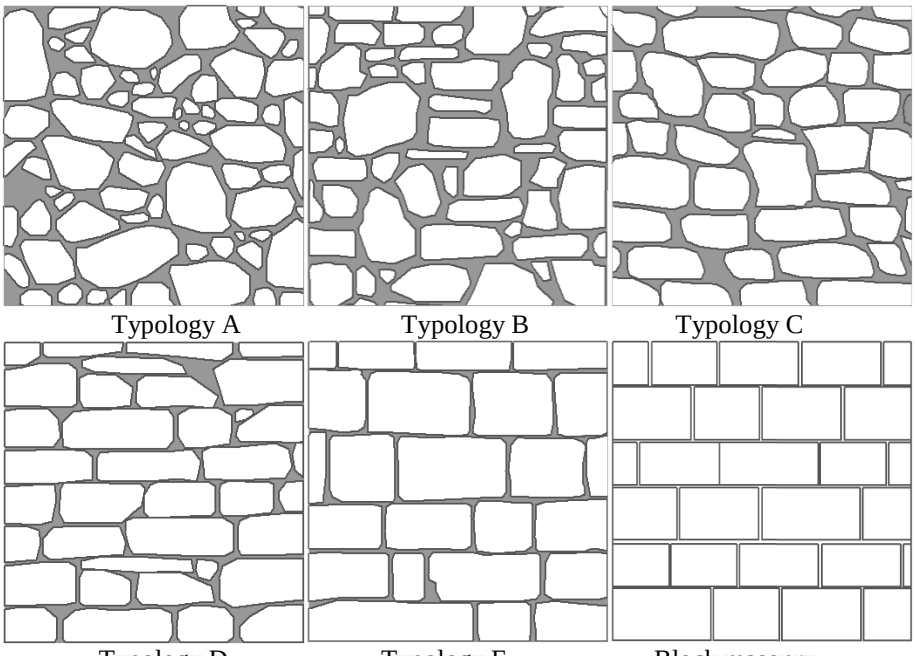

Figure 1. Patterns of five stone masonry topologies that are defined by the Italian code (MIT 2009) and a block masonry pattern. Sketches from Vanin et al. (2017).

While we might sense that from Typology A to E, material strength should increase, the Line of Minimum Trace (LMT) (Doglioni et al. 2009) can be used for quantifying the level of interlocking.

$$\text{LMT} = \frac{\text{Min. trace though joints}}{h_v} \tag{15}$$

In practice, LMT is one criteria for determining the Masonry Quality Index (MQI) (A Borri and Maria 2009; Antonio Borri et al. 2015). Currently, calculation of LMT requires hand tracing the masonry pattern which is time consuming and sometimes leads to objective results.

3.2 Masonry Typology Generator

As indicated in the introduction, one corner stone which was missing is the ability to systematically generate stone patterns for each typology. Here in this subsection, we introduce the micro structure generator recently proposed (Zhang et al. 2017a). The construction of the masonry typology can be divided into two stages, i.e., the construction of a joint pattern, which leads to a cellular structure such that each stone is contained in a single cell, and an erosion process to create the mortar layer.
The first stage is illustrated in Figure 2 and Figure 3. The basic joint pattern is created by laying down stone by stone, from bottom to top, from left to right. Figure 2a presents one basic joint pattern after laying down the first layer. Starting from the second layer, the bottom left corner of each new stone corresponds to the bottom right corner of the previous stone. As a result, the stone could be overhanging or overlapping on the right side. To solve this problem, two different approaches for continuing the joint pattern generation have been proposed (Zhang et al. 2017a). Apart from the stone-placing technique described above, we introduce a new stone-pattern-generation option that uses Voronoi cells (Voronoi 1908). As illustrated by Figure 3a, Voronoi cells can be used to generate patterns for a whole region, which is more representative when the region is totally unstructured (e.g., rubble masonry), or split selected stones (e.g. stones with an area that is larger than a specified threshold value).

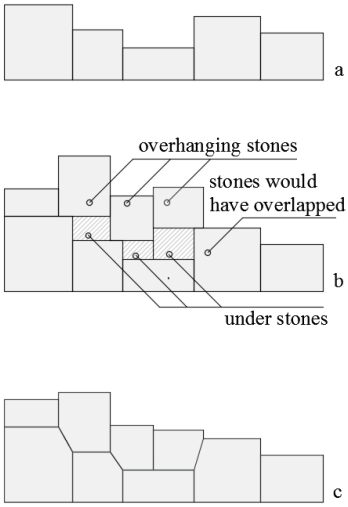

Figure 2. Illustration of the construction of joint pattern (Zhang et al. 2017a).

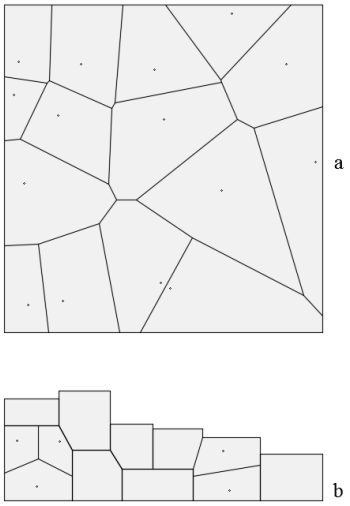

Figure 3. Voronoi spliting of stones.

The joint pattern created above is suitable for the simplified-micro modeling approach where mortar layers are represented by zero thickness interface elements (Louren ço 1996; Senthivel and Louren ço 2009; Snozzi and Molinari 2013). To create a mortar layer of non-uniform thickness and rounded stones edges, we use the weathering algorithm in Jones et al. (2010) that was originally developed to simulate the wind erosion of rocks. The outcome of the erosion process for a single stone is shown in Figure 4. The joint boundary of the stone prior to the erosion process is indicated in red, with the blue line indicating the eroded boundary of the stone.

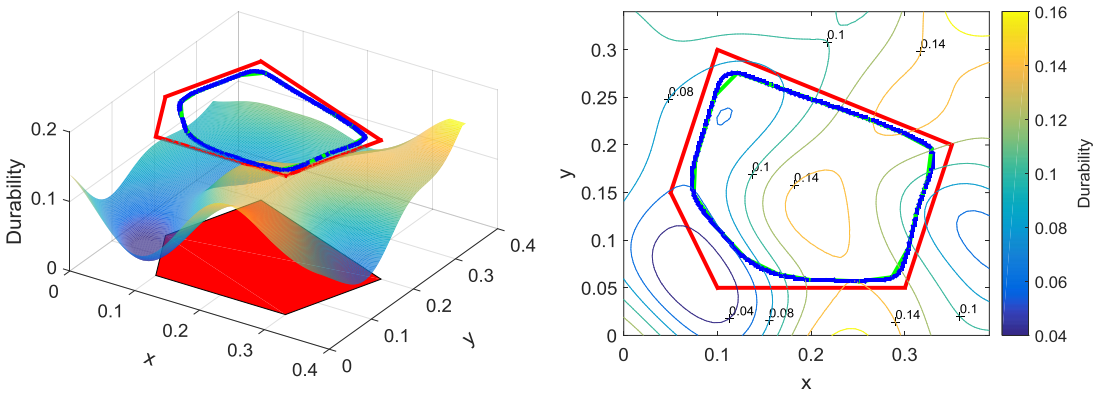

(a) one sample of random durability (b) corresponding eroded stone boundary

Figure 4. The erosion process and sampling of boundary points.

By using the above-mentioned procedure, three samples are generated for each topology (Figure 5). As shown in Figure 5, a large variety of masonry topologies with characteristics corresponding to those of the typical patterns can be generated using the micro-structure generator. The parameters chosen for the generation of the patterns are available online together with the code of the micro-structure generator (Zhang et al. 2017a).

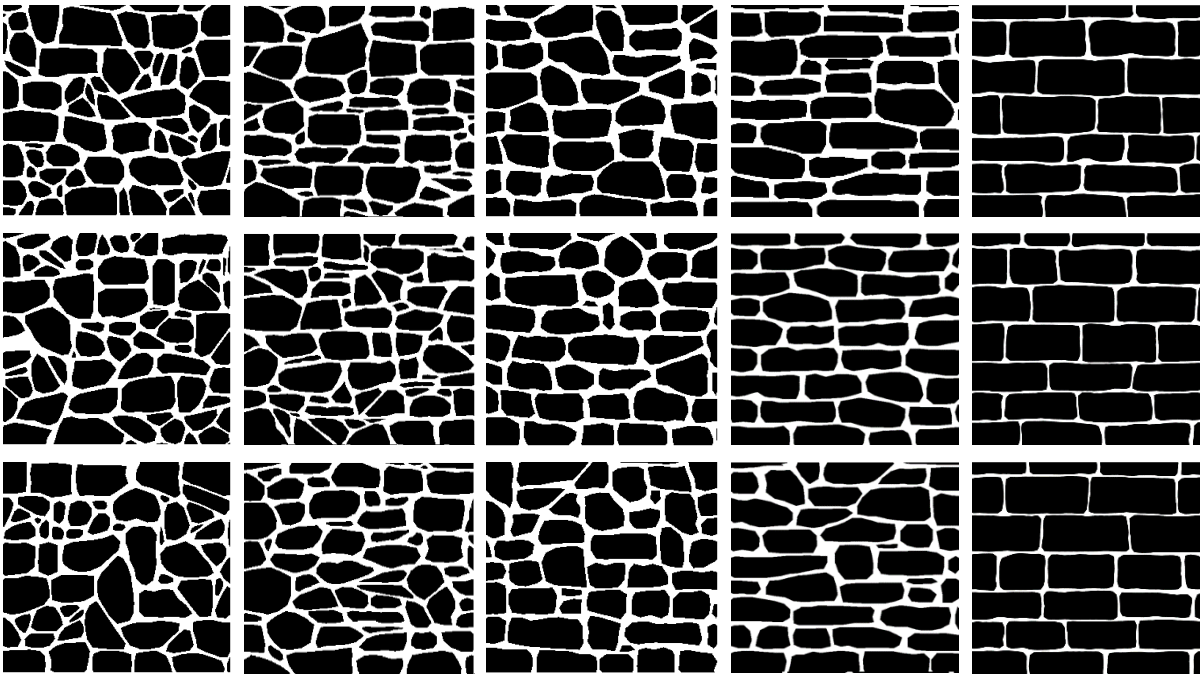

Typology A Typology B Typology C Typology D Typology E

Figure 5. Generated samples for five topologies of the Italian code.

3.3 Calculation of the Line of Minimum Trace

As indicated before, the quantification of interlocking can be associated with the LMT. To facilitate the calculation of the LMT, here we rewrite the definition of LMT (Equation (15)) in a discrete version. Without loss of generality, let point $\boldsymbol{p}_1 = \boldsymbol{p}_{\text{start}}$ be the starting point and $\boldsymbol{p}_{\text{n}} = \boldsymbol{p}_{\text{end}}$ be the ending point. The straight line distance between $\boldsymbol{p}_{\text{start}}$ and $\boldsymbol{p}_{\text{end}}$ is indicated by $\|\boldsymbol{p}_{\text{start}} - \boldsymbol{p}_{\text{end}}\|$. In the case $\boldsymbol{p}_{\text{start}}$ and $\boldsymbol{p}_{\text{end}}$ lie along the same vertical line, we would have $h_v = \|\boldsymbol{p}_{\text{start}} - \boldsymbol{p}_{\text{end}}\|$ as in Equation (15).

The minimum trace through joints is calculated as follows. Define the path between two points $\boldsymbol{p}_1$ and $\boldsymbol{p}_{\text{n}}$ as a sequence of vertices $\text{P} = (\boldsymbol{p}_1, \boldsymbol{p}_2, \dots, \boldsymbol{p}_{\text{n}})$ such that $\boldsymbol{p}_{\text{i}}$ is visible to $\boldsymbol{p}_{\text{i+1}}$ for $1 \le i \le n-1$. If we

call $\boldsymbol{e}_{\mathrm{i,i+1}}$ the edge connecting $\boldsymbol{p}_{\mathrm{i}}$ and $\boldsymbol{p}_{\mathrm{i+1}}$, and we define a weight function $d(\boldsymbol{e}_{\mathrm{i,i+1}})$, the shortest path between $\boldsymbol{p}_{\mathrm{start}}$ and $\boldsymbol{p}_{\mathrm{end}}$ is defined as the path $\mathrm{P} = (\boldsymbol{p}_1, \boldsymbol{p}_2, \dots, \boldsymbol{p}_{\mathrm{n}})$ with $\boldsymbol{p}_1 = \boldsymbol{p}_{\mathrm{start}}$, $\boldsymbol{p}_{\mathrm{n}} = \boldsymbol{p}_{\mathrm{end}}$, which minimizes the $\sum_{i=1}^{n-1} d(\boldsymbol{e}_{\mathrm{i,i+1}})$ $\forall \mathrm{n}$. The parameter LMT is defined as the total distance of the shortest path divided by the straight line connecting the start and end points (Equation 1), which is

$$\mathrm{LMT} = \frac{\sum_{i=1}^{n-1} d(\boldsymbol{e}_{\mathrm{i,i+1}})}{\|\boldsymbol{p}_{\mathrm{start}} - \boldsymbol{p}_{\mathrm{end}}\|} \tag{16}$$

The detailed calculation procedure is detailed in Zhang et al. (2017a). With the definition in Equation (16), it is possible to consider the fact that most of the cracks follow the interface because that the interface is much weaker than the mortar itself. To do this, we define $d(\boldsymbol{e}_{\mathrm{i,i+1}}) = \alpha\|\boldsymbol{p}_{\mathrm{i+1}} - \boldsymbol{p}_{\mathrm{i}}\|$, $0 < \alpha \leq 1$ indicates traveling along the interface is easier, thus the path tends to follow the interface, while $\alpha = 1$ gives that traditional definition of LMT. An illustration of the shortest path is given by Figure 6. The LMTs for shortest path of all the samples in Figure 1 and Figure 5 are shown in Figure 7, from which it can be seen that the level of interlocking increases from typology A to typology E.

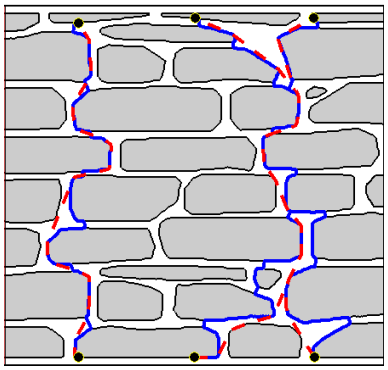

Figure 6. Illustration of shortest path for different α
(The blue lines correspond to α=0.1 and the red lines to α=1.0) (Zhang et al. 2017a).

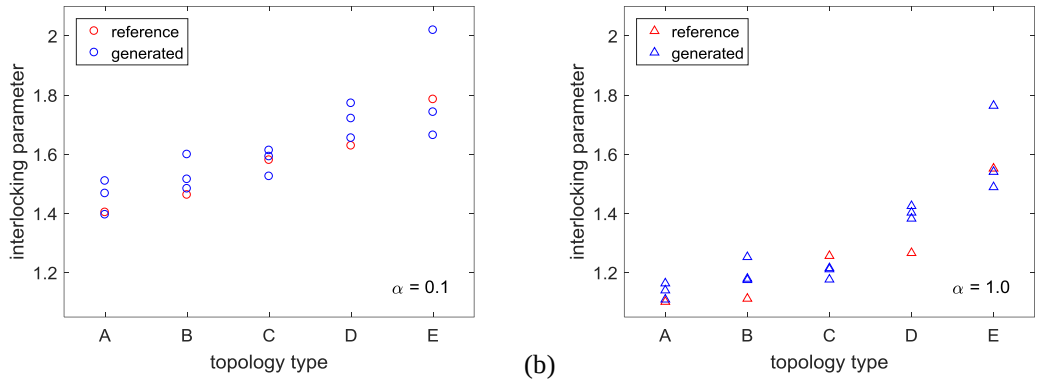

Figure 7. Comparision of the line of minimum trace of topologies A to E for α=1.0 (a) and α=0.1 (b) (Zhang et al. 2017a).

4. NUMERICAL EXAMPLE

The previous section presented the micro-structure generator and gave a geometrical analysis for the samples generated. We have seen from Figure 7 that we did have an increase of LMT while the typology changes from A to E. A question arises naturally, do we also have an increase with regard to material strength? In this section, we answer this question by analyzing the samples under various boundary conditions, compression and shear-compression using the detailed micro-model introduced in Section 2. The material properties chosen for the simulation are listed in Table 1 and Table 2.

Table 1. Elastic properties.

Material	Young Modulus (MPa)	Poisson ratio	Density
Stone	20 200	0.2	2 600
Mortar	500	0.2	1 800

Table 2. Inelastic properties.

	f_t (MPa)	c (MPa)	G_c^I (N/m)	G_c^{II} (N/m)	μ
Stone	1.00	2.00	1 000	10 000	0.65
Mortar	0.15	0.30	30	300	0.65
Interface	0.05	0.10	10	100	0.65

4.1 Compression test

The compressive strengths obtained from the simulation are summarized in Figure 8. When the typology changes from A to E, assumiung that the material properties remain the same, the mean compressive strength increases from 1.06 to 5.78 MPa. The compressive strength values obtained corresponds well with the range of values given by the Italian code, which for Typology A is 1.00-1.80 MPa and for Typology E is 6.00-8.00 MPa (Table C8A.2.1 in MIT (2009)). The typical failure mode for each typology is shown in Figure 9. With the increase of LMT, the failure mode changes from inter-facial damage to damage passing through the stones, which explains the signicant increase of the compressive strength. The relation between compressive strength and LMT is shown in Figure 10, which indicates a positive correlation between LMT and compressive strength.

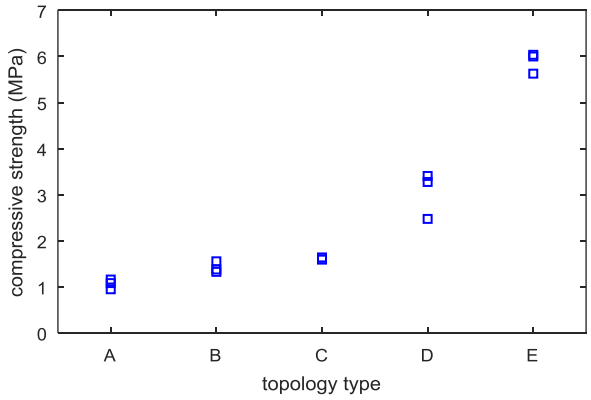

Figure 8. Comparison of compressive strengths for different typologies.


Typology A Typology B Typology C Typology D Typology E

Figure 9. Typical crack patterns for different topologies under compression.

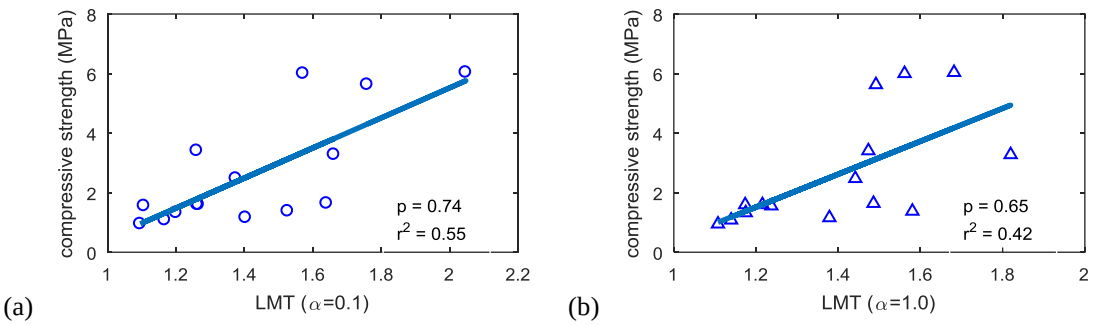

Figure 10. Relation between compressive strength and LMT (for different α).

4.2 Shear Compression test

In this subsection, we simulate shear walls of different typologies subjected to combined axial compression and lateral shear loading. To apply the axial force, a loading beam is added on top of the specimen and a force boundary condition is applied on top of the beam. Two different compression levels are applied: a low compression $\sigma_n = 0.1$ MPa and a moderate compression $\sigma_n = 0.5$ MPa. During the test, the loading beam is pushed from left to right. The loading protocol is similar to what has been used in the experimental tests by Vasconcelos (2005).

For shear test under low compression, the maximum shear strengths for different specimens are listed in Figure 11. It can be seen that in general the global strength obtained is smaller than the cohesion of the interface (0.01 MPa). Figure 11 also reveals that there has been a gradual decrease in the variability of the shear strength while the typology changes from A to E. The typical failure patterns are given in Figure 12. The graphs show that a flexural failure type is favored under this low compression level and the cracks tend to follow the horizontal interface, thereby explaining the low variability of shear strengths obtained for typology D and E, where the horizontal interface is straight and the variation is small. An examination of the Pearson's linear correlation coefficient (indicated by p, $p = 0.02$ for $\alpha = 0.1$ and $p = 0.04$ for $\alpha = 1.0$, Figure 13) indicates no correlation between LMT and (flexual) shear strength since $p<0.05$.

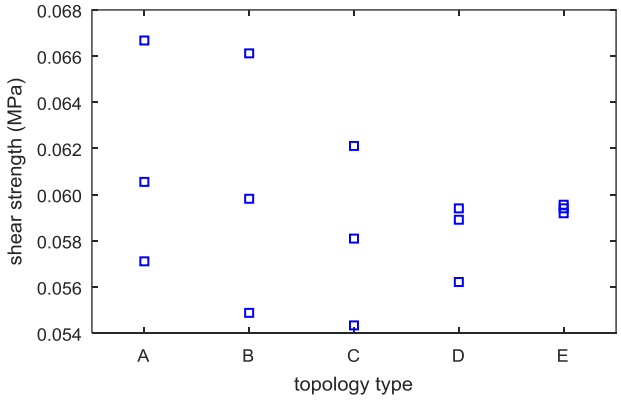

Figure 11. Comparison of shear strengths for different typologies ($\sigma_n = 0.1$ MPa).

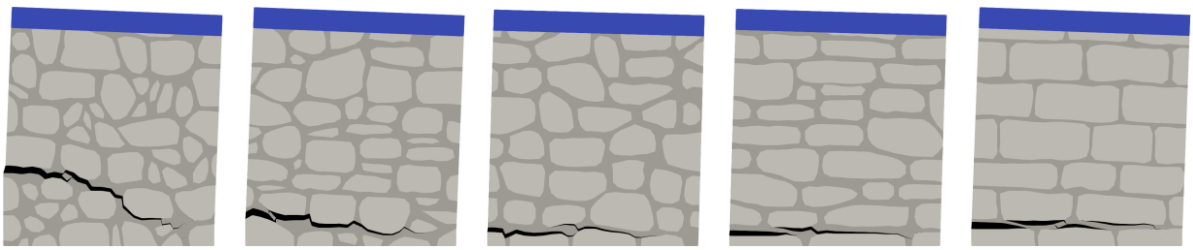

Typology A Typology B Typology C Typology D Typology E

Figure 12. Typical crack patterns for different topologies under shear compression ($\sigma_n = 0.1$ MPa).

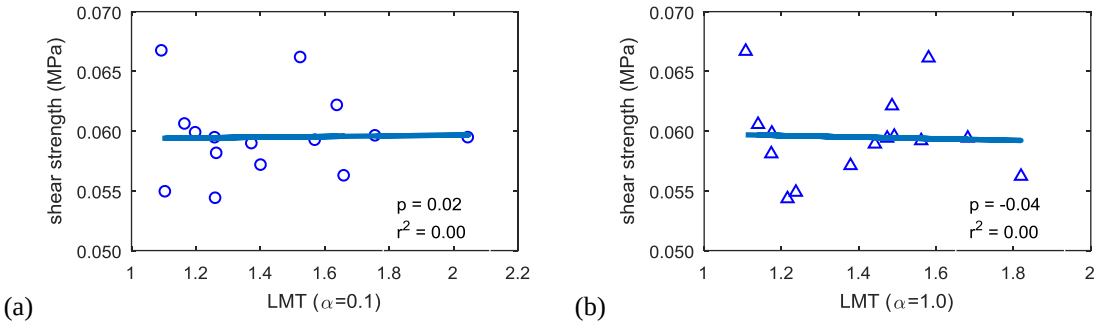

Figure 13. Relation between shear strength and LMT ($\sigma_n = 0.1$ MPa).

While the compression level increases from 0.1 MPa to 0.5 MPa, the shear strengths also increase significantly as shown in Figure 14. What stands out in the figure is that now we observe a gradual increase of shear strength while typology changes from A to E. Specifically, the mean shear strength for typology A is 0.163 MPa and for typology E is 0.212 MPa, from which a 30 % increase is observed. The typical crack patterns under this compression level are shown in Figure 15. A mixed failure type of compression and shear is observed. A positive correlation was found between shear strength and LMT. As shown in Figure 16, for $\alpha = 0.1$, Pearson's linear correlation coefficient is $p = 0.58$ and the coefficient of determination $r^2 = 0.33$, while for $\alpha = 1.0$, $p = 0.61$ and $r^2 = 0.37$.

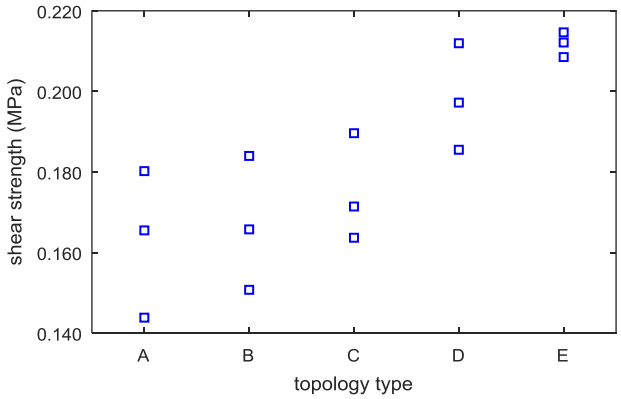

Figure 14. Comparison of shear strengths for different typologies ($\sigma_n = 0.5$ MPa).

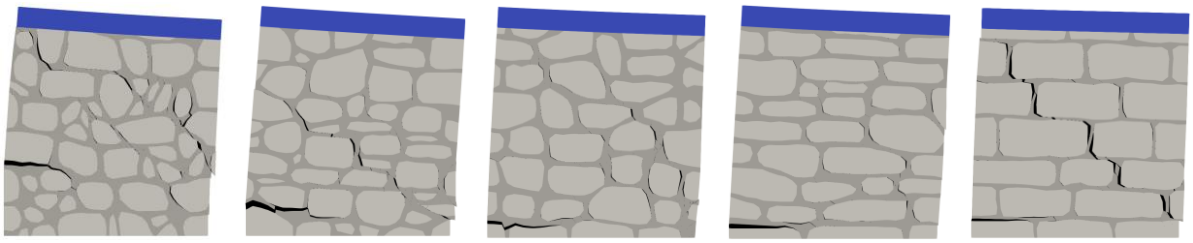

Typology A Typology B Typology C Typology D Typology E

Figure 15. Typical crack pattern for different topologies under shear compression ($\sigma_n = 0.5$ MPa).

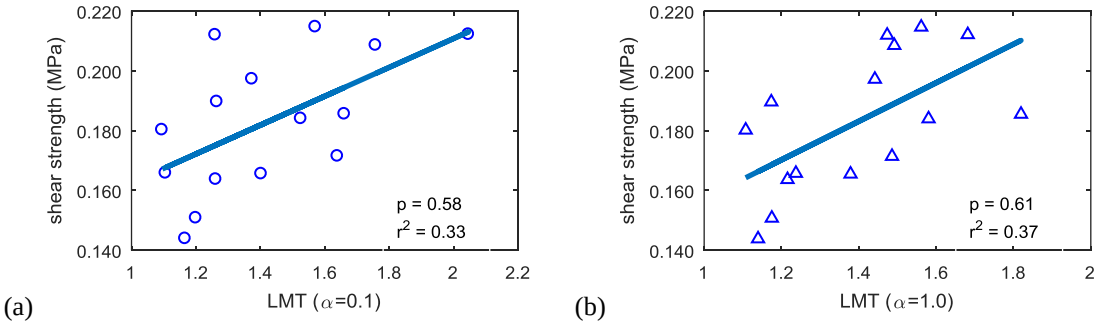

Figure 16. Relation between shear strength and LMT ($\sigma_n = 0.5$ MPa).

5. CONCLUSION

This paper is the first study to investigate the effect of typology on masonry strength for stone masonry. After introducing the numerical simulation framework and summarizing the proposed typology generator, we analyzed the compressive and shear strength for different typologies. The study has shown that typology has a significant influence on material strength. The validity of LMT as an indicator of the material strength depends on the boundary condition or, more specifically, the failure mode. A positive correlation between LMT and shear/compression strength is observed, while the flexural strength is totally uncorrelated with the LMT. These findings enhance our understanding of the mechanical behavior of stone masonry and the influence of interlocking on irregular masonry. Future research includes the study of the strength domain for a larger range of loading conditions and the dependence of the drift capacity on the masonry topologies.

6. ACKNOWLEDGMENTS

This study was supported by the Swiss National Science Foundation through the grant 20 0 021_140973/1.

7. REFERENCE

Borri A, Corradi M, Castori G, De Maria A (2015). A method for the analysis and classification of historic masonry. *Bulletin of Earthquake Engineering*, *13*(9): 2647–2665. https://doi.org/10.1007/s10518-015-9731-4

Borri A, De Maria A (2009). L'indice di qualità muraria (IQM): Evoluzione ed applicazione nell'ambito delle norme tecniche per le costruzioni del 2008. *Proceedings of 13th Italian National Conference for …*.

Camacho GT, Ortiz M (1996). Computational modelling of impact damage in brittle materials. *International Journal of Solids and Structures*, *33*(20): 2899–2938.

D'Ayala D, Speranza E (2003). Definition of collapse mechanisms and seismic vulnerability of historic masonry buildings. *Earthquake Spectra*, *19*(3): 479–509. https://doi.org/10.1193/1.1599896

Doglioni F, Mirabella Roberti G, Bondanelli M (2009). *Definizione della Linea di Minimo Tracciato come elemento per la qualifica dell'ingranamento nel piano e fuori dal piano, Prodotto final Linea 1, progetto Reluis*.

Grünthal G (1993). *European Macroseismic Scale 1992 (EMS-92). Cahiers du Centre Européen de Géodynamique et de …*. Luxembourg.

Jones MD, Farley M, Butler J, Beardall M (2010). Directable Weathering of Concave Rock Using Curvature Estimation. *IEEE Transactions on Visualization and Computer Graphics*, *16*(1): 81–94. https://doi.org/10.1109/TVCG.2009.39

Kržan M, Gostič S, Cattari S, Bosiljkov V (2015). Acquiring reference parameters of masonry for the structural performance analysis of historical buildings. *Bulletin of Earthquake Engineering*, *13*(1): 203–236. https://doi.org/10.1007/s10518-014-9686-x

Lourenço PB (1996). *Computational strategies for masonry structures*. *PhD Thesis*. Delft University of Technology. https://doi.org/ISBN 90-407-1221-2

Milani G, Lourenço PB, Tralli A (2006). Homogenised limit analysis of masonry walls, Part I: Failure surfaces. *Computers & Structures*, *84*(3–4): 166–180. https://doi.org/10.1016/j.compstruc.2005.09.005

MIT (2009). *Ministry of Infrastructures and Transportation, Circ. C.S.Ll.Pp. No. 617 of 2/2/2009: Istruzioni per l'applicazione delle nuove norme tecniche per le costruzioni di cui al Decreto Ministeriale 14 Gennaio 2008, G.U.S.O. n.27 of 26/2/2009, No. 47, 2008 (in* .

Pina-Henriques JL (2005). *Masonry under Compression: Failure Analysis and Long-Term Effects*. PhD thesis, University of Minho, Portugal, Guimaraes.

Roca P, Cervera M, Gariup G, Luca P, Pela' L, Luca P, Pelà L (2010). Structural Analysis of Masonry Historical Constructions. Classical and Advanced Approaches. *Archives of Computational Methods in Engineering*, *17*(3): 299–325. https://doi.org/10.1007/s11831-010-9046-1

Senthivel R, Lourenço PB (2009). Finite element modelling of deformation characteristics of historical stone masonry shear walls. *Engineering Structures*, *31*(9): 1930–1943. https://doi.org/10.1016/j.engstruct.2009.02.046

Shieh-Beygi B, Pietruszczak S (2008). Numerical analysis of structural masonry: mesoscale approach. *Computers & Structures*, *86*(21–22): 1958–1973. https://doi.org/10.1016/j.compstruc.2008.05.007

Snozzi L, Molinari J-F (2013). A cohesive element model for mixed mode loading with frictional contact capability. *International Journal for Numerical Methods in Engineering*, *93*(5): 510–526.

Vandoren B, De Proft K, Simone A, Sluys LJ (2013). Mesoscopic modelling of masonry using weak and strong discontinuities. *Computer Methods in Applied Mechanics and Engineering*, *255*: 167–182. https://doi.org/10.1016/j.cma.2012.11.005

Vanin F, Zaganelli D, Penna A, Beyer K (2017). Estimates for the stiffness, strength and drift capacity of stone masonry walls based on 123 quasi-static cyclic tests reported in the literature. *Bulletin of Earthquake Engineering*, (12): 5435–5479. https://doi.org/10.1007/s10518-017-0188-5

Vasconcelos GFM (2005). *Experimental investigations on the mechanics of stone masonry : characterization of granites and behavior of ancient masonry shear walls*. University of Minho, Guimaraes. Retrieved from http://repositorium.sdum.uminho.pt/handle/1822/17383

Voronoi G (1908). Nouvelles applications des paramètres continus à la théorie des formes quadratiques. Deuxième mémoire. Recherches sur les parallélloèdres primitifs. *Journal für die reine und angewandte Mathematik*, *134*: 198–287. Retrieved from https://eudml.org/doc/149291

Zhang S, Hofmann M, Beyer K (2017a). A 2D typology generator for historical masonry elements. *Construction and Building Materials (Submitted)*.

Zhang S, Taheri Mousavi SM, Richart N, Molinari J-F, Beyer K (2017b). Micro-mechanical finite element modeling of diagonal compression test for historical stone masonry structure. *International Journal of Solids and Structures*, *112*: 122–132. https://doi.org/10.1016/j.ijsolstr.2017.02.014